Anomalous Nonlinear Optical Response of Graphene Near Phonon Resonances

Lucas Lafetá,[†] Alisson R. Cadore,[†] Thiago G. Mendes-de-Sa,[†] Kenji Watanabe,[‡] Takashi Taniguchi,[‡] Leonardo C. Campos,[†] Ado Jorio,[†] and Leandro M. Malard*,[†]

[†]Departamento de Física, Universidade Federal de Minas Gerais, Belo Horizonte, Minas Gerais 31270-901, Brazil
[‡]National Institute for Materials Science (NIMS), 1-2-1 Sengen, Tsukuba-city, Ibaraki 305-0047, Japan

Ⓢ Supporting Information

ABSTRACT: In this work we probe the third-order nonlinear optical property of graphene and hexagonal boron nitride and their heterostructure by the use of coherent anti-Stokes Raman spectroscopy. When the energy difference of the two input fields matches the phonon energy, the anti-Stokes emission intensity is enhanced in h-BN, as usually expected, while for graphene an anomalous decrease is observed. This behavior can be understood in terms of a coupling between the electronic continuum and a discrete phonon state. We have

also measured a graphene/h-BN heterostructure and demonstrate that the anomalous effect in graphene dominates the heterostructure nonlinear optical response.

KEYWORDS: Nonlinear optics, graphene, hexagonal boron nitride, four-wave mixing
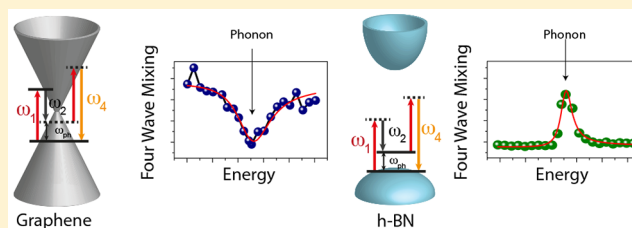
Two-dimensional materials like graphene, hexagonal boron nitride (h-BN), and heterostructures exhibit novel physical properties and promise different applications in electronics and photonics.[1−4] Nonlinear optical phenomena like second- and third-harmonic generation and four-wave mixing (FWM)[5−7] can be quite strong in these materials.[8−18] However, the interpretation of the nonlinear optical response is strongly affected by electronic and phonon resonances;[19−22] therefore, the knowledge of the interplay between these resonances is desirable. Here we measured the third-order optical emission by the degenerated four-wave mixing emission of graphene, h-BN, and their heterostructure near phonon resonances. We show that, while the FWM signal in h-BN shows the expected enhancement, in graphene the signal is decreased exactly at the phonon resonance. Because graphene is a zero gap semiconductor, while h-BN is an insulator, we explain our results in terms of interference effects between the electronic and the phonon states for these two different materials. Moreover, we characterized the third-order nonlinear sheet susceptibility of h-BN and find that it is 1 order of magnitude smaller than in graphene. This result is corroborated by our observation that in a graphene/h-BN heterostructure the graphene signal dominates the nonlinear optical response.

Four-wave mixing is a third-order nonlinear optical phenomena, where three frequencies are combined to generate a fourth.[7] In this work we are restricted to the case of degenerate FWM, where two photons of frequency ω_1 combine with a photon of ω_2 at the material and generate the emission of another photon with frequency ω_4. The energy conservation in this case is given by $\hbar\omega_4 = 2\hbar\omega_1 - \hbar\omega_2$. Hendry et al.[8] have measured the FWM intensity in graphene as a function of the

pump laser energy, and its third-order optical nonlinear optical property was characterized. Also different theoretical works have calculated the third-order optical conductivity of graphene,[23−27] showing the importance of different physical quantities like Fermi energy or temperature. However, these works did not treat the problem of the third-order optical nonlinearity near phonon resonances. The so-called coherent anti-Stokes Raman spectroscopy (CARS) is a special case of FWM when the energy difference between $\hbar\omega_1$ and $\hbar\omega_2$ matches a phonon energy ($\hbar\omega_{ph}$); then ω_4 corresponds exactly to the anti-Stokes frequency in Raman scattering. In general, when the energy condition $\hbar\omega_1 - \hbar\omega_2 = \hbar\omega_{ph}$ is satisfied, the ω_4 amplitude is enhanced.[19−22]

To study the CARS phenomenon in graphene and h-BN, flakes were prepared by micromechanical cleavage of natural graphite or bulk h-BN on transparent quartz substrates (SPI Inc.). Monolayer graphene was identified in the substrates by an optical microscope followed by Raman characterization, where the 2D Raman band in monolayer graphene was characterized by a single Lorentzian.[28] The h-BN flakes used were few layers (10−20 layers estimated from optical contrast[29]). For the CARS experiment we have used an optical parametric oscillator system (APE PicoEmerald) with 6 ps pulse width and 76 MHz repetition rate. This laser system emits two collinear laser beams with frequencies ω_1 and ω_2. The frequency ω_1 can be tuned between 720 and 960 nm in

steps of 0.5 nm, and the second ω_2 is fixed at 1064 nm. Both laser beams are spatially and temporally overlapped and focused at the sample by a 60× and 0.95 N.A. objective. The backscattered signal is collected by the same objective, reflected by a beam splitter (BS), filtered by a short pass (SP) to remove the pump wavelengths, and directed to a single grating spectrometer equipped with a CCD camera (see schematics in Figure 1a). Raman spectra were acquired in the same setup, but using a 561 nm diode laser with an edge filter in front of the spectrometer (bottom panel in Figure1b,c).

Figure 1b shows the CARS spectrum (ω_4 intensity as a function of ω_1 wavelength) in few layer h-BN deposited on quartz substrate. The ω_4 intensity is enhanced when the pump wavelength ω_1 is around 929 nm. Converting the bottom scale to $\hbar\omega_2 - \hbar\omega_1$ in wavenumbers (top scale), the enhancement in
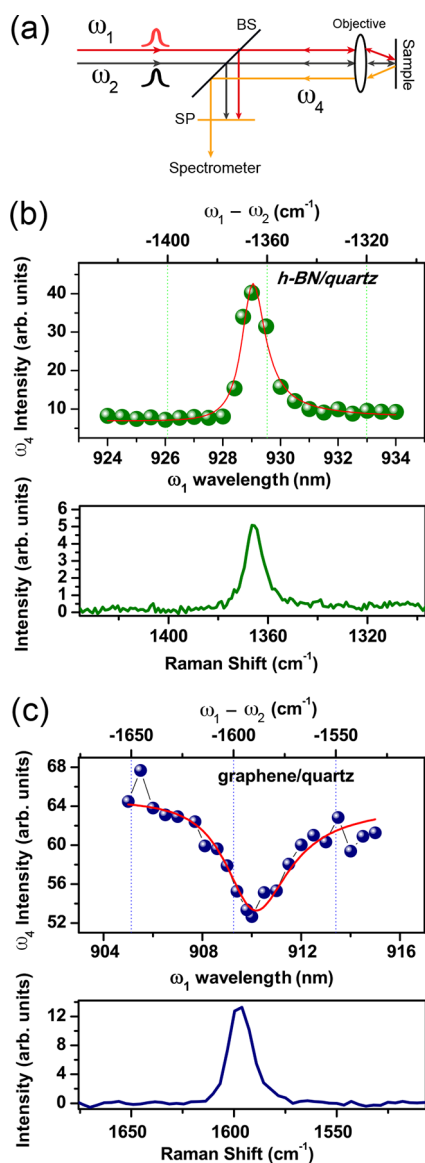
Figure 1. (a) Experimental setup, showing the two pump beams with frequencies ω_1 and ω_2. (b) CARS intensity as a function of the ω_1 pump wavelength (bottom scale) or $\hbar\omega_2 - \hbar\omega_1$ in wavenumbers (top scale) for few layer h-BN. The solid red lines is the fit from the theory described in text. The graph bellow shows the Raman spectrum taken at the same energy range. (c) Same as (a) but for the monolayer graphene sample.

CARS intensity happens exactly at 1366 cm^{-1}, which corresponds to the double-degenerate in-plane optical phonon mode in h-BN. To further verify this assignment, the sample is measured by linear Raman spectroscopy as shown in the Raman spectrum at the bottom plot of Figure 1b.

Figure 1c shows the measurement of a monolayer graphene deposited on a similar quartz substrate and, surprisingly, the nonlinear optical behavior is the opposite; that is, the CARS intensity decreases when the pump wavelength is ~910 nm. Again, converting the bottom scale to $\hbar\omega_2 - \hbar\omega_1$, we verify that the observed antiresonance in the ω_4 intensity is centered at the 1590 cm^{-1} peak, which is the energy of the double-degenerate in-plane optical phonon mode in graphene (G band). This assignment is confirmed by the Raman spectrum of the same monolayer graphene sample shown in Figure 1c, bottom plot.

The ω_4 emission intensity (I_{ω_4}) in a CARS process depends on the intensity of ω_1 (I_{ω_1}) and ω_2 (I_{ω_2}) and on the frequency-dependent third-order nonlinear susceptibility $\chi^{(3)}(\omega)$ as $I_{\omega_4} \propto |\chi^{(3)}(\omega)|^2 \, I_{\omega_1}^2 I_{\omega_2}$.[7,30] It is also important to note that the ω_4 amplitude is also dependent on the momentum conservation,[6,7,31] which is not included in the previous equation. This is justified because in our experimental setup we use collinear beam excitation, tight focusing (large N.A. objective), and a sample thickness much smaller than the light wavelength. In such case it was shown that the forward and backward CARS signals have similar intensities.[32,33] In a simple analysis, where only electronic virtual states are present, the $\chi^{(3)}(\omega)$ is a function with real and complex parts. The real function describes the so-called nonresonant background due to light absorption by virtual electronic states. The imaginary function describes a resonant state due to transition between virtual excited electronic states to a discrete phonon state.[7,30] As shown before (ref 30 and references therein) this simple analysis describes well the CARS spectrum for different transparent materials and molecules. However, such model cannot explain the antiresonance behavior observed for graphene, as shown in Figure 1c.

The CARS process obeys $\omega_4 = 2\omega_1 - \omega_2$, as shown in Figure 2. h-BN is a insulator with a band gap energy higher than the laser energies used in this work;[34] therefore, the pump photon ω_1 makes a first transition from the ground state to a virtual excited state, followed by a transition induced by the ω_2 photon to a real phonon state (see Figure 2a). Another ω_1 photon makes a transition from the phonon state to a virtual state, and the ω_4 photon is created by decaying from the second virtual state to the ground state. Therefore, for h-BN the CARS process connects only virtual electronic states and a real phonon state when the energy condition $\hbar\omega_1 - \hbar\omega_2 = E_{ph}$ is satisfied. This is the usual CARS process, and it can be described by the $\chi^{(3)}(\omega)$ function as discussed in the previous paragraph.

The situation is different in monolayer graphene, which is a zero gap semiconductor, where the valence and conduction bands touch each other at the K and K′ points of the Brillouin zone. Several works have addressed the calculation of $\chi^{(3)}$ as a function of energy for graphene;[23−26] however, the influence of discrete phonon states are still lacking in the literature. In Figure 2b the same CARS process is depicted; however, in this case all of the excited electronic states involved can be real, and resonance can be always achieved, not only in the four optical processes but also within the phonon ω_{ph} energy. Therefore,
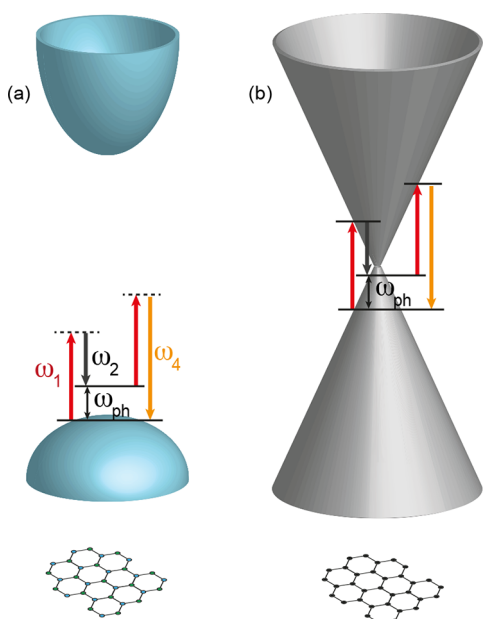
Figure 2. (a) h-BN band structure with a possible CARS process, where the two pump beams with frequencies ω_1 and ω_2 are combined to generate the emission of photons with frequency ω_4 obeying $\omega_1 - \omega_2 = \omega_{\text{ph}}$. (b) The same as (a) but for graphene.

the $\chi^{(3)}(\omega)$ of graphene will be comprised by a sum of several terms, each one responsible for the different optical resonances with electronic transitions in graphene and another term responsible to describe the resonance with the phonon state. Differently from h-BN where the electronic transitions are absent, in graphene the $\chi^{(3)}(\omega)$ will have contributions both from electronic and phonon states.

The graphene case is similar to the work of Nestor et al.[35] where the CARS spectrum with pump lasers close to electronic transitions were studied. By tuning the pump laser wavelength near the absorption peak of vitamin B_{12}, Nestor et al. showed that it was possible to observe a transition between a resonance to antiresonance profile in the CARS spectra. Theoretical efforts have been made to treat this problem,[7,36,37] and its explanation involves the calculation of $\chi^{(3)}$ where multiple terms are exhibited depending on the resonant conditions between electronic and phonon states.[7,36,37] Since the final CARS intensity is proportional to $|\chi^{(3)}|^2$, interference effects can occur and modify the CARS line shape. Another approach[38] is to realize that $\chi^{(3)}$ is comprised by a sum of a continuum of electronic contributions and a discrete phonon state, and these two terms can interfere with each other depending on their relative weight. Such methodology has been applied to understand the FWM[39,40] and CARS spectra of atomic systems at high energies[38] where the nonlinear emission intensity was described by the phenomenological Fano line shape.[41] The Fano line shape is useful for describing systems where it was possible to observe interference effects between electronic continuum and discrete states. Therefore, to understand our results we will describe the CARS intensity of both h-BN and graphene with the Fano line shape as a function of energy E, as

$$I_{\omega_4}(E) = A\frac{[(E - E_{\text{ph}}) + \gamma q]^2}{(E - E_{\text{ph}})^2 + \gamma^2} \tag{1}$$

where A is a proportionality constant, E is the energy difference between the pump beams ($\hbar\omega_1 - \hbar\omega_2$), E_{ph} is the phonon

energy, γ the phonon state broadening, and q is a dimensionless parameter that gives the overall contribution between an electronic continuum or a discrete phonon state for the FWM intensity. If $|q| = 1$ there is an equal weight contribution between the electronic continuum and discrete phonon state. If $|q| \ll 1$ there is a larger contribution to the electronic continuum, and if $|q| \gg 1$ the contribution mainly comes from the discrete phonon state. When the phonon discrete state dominates ($|q| \gg 1$), there is a resonance line shape, and the profile is similar to the usual CARS profess. When the electronic continuum dominates ($|q| \ll 1$), however, there is an antiresonance line shape. We have used eq 1 to fit our experimental results in Figure 1. For h-BN, the q value found is -6 (discrete phonon state dominates) giving rise to a resonant behavior of the CARS spectrum at the phonon energy. On the other hand, the value found for q in monolayer graphene is 0.09 (continuum electronic states dominates) which leads to the antiresonance CARS line shape behavior at the phonon energy. Based on this Fano analysis our results can now be understood: in graphene the electronic contributions are expected to play a major role due to the absence of an optical gap; that is, there is a continuum of optical resonances. Therefore, in graphene the CARS intensity presents an antiresonance behavior exactly at the phonon energy. In contrast, in h-BN the optical gap is much larger than the energies used in our experiment; therefore, we expect very low contribution from the electronic states, and the CARS intensity is a resonance peak located exactly at the phonon energy.

From the fitting we can also extract the phonon line width γ, which serves as an internal consistency analysis. For graphene γ is found to be equal 12 cm^{-1} is in agreement with value measured from Raman spectroscopy of 11 cm^{-1} (Figure 1c), and in agreement with the literature.[28] For h-BN we have found $\gamma = 8$ cm^{-1}, which is close to our experimental resolution of 6 cm^{-1} for CARS experiment, but in agreement with the value found for Raman spectroscopy of 9 cm^{-1} (Figure 1b).

Lets us focus on the characterization of the nonlinear third-order susceptibility $\chi^{(3)}$ for both graphene and h-BN. We have measured the four-wave mixing intensity for both materials and normalized it by a fused quartz reference sample (more details in the Supporting Information). For graphene the value of the sheet third-order nonlinear susceptibility found in our experiment is $\chi^{(3)}_{\text{sheet}} = (9 \pm 1) \times 10^{-30}$ m^3/V^2 out from the phonon resonance and $\chi^{(3)}_{\text{sheet}} = (5 \pm 1) \times 10^{-30}$ m^3/V^2 at the phonon resonance. This is $\sim$5 times smaller than the value found by Woodwart et al.[17] of $\chi^{(3)}_{\text{sheet}} = (50 \pm 1) \times 10^{-30}$ m^3/V^2. However, the values reported in the literature differs in orders of magnitude depending on the measurement type, sample, and light wavelength.[42] For h-BN we find $\chi^{(3)}_{\text{sheet}} = (9 \pm 1) \times 10^{-31}$ m^3/V^2 out from the phonon resonance and $\chi^{(3)}_{\text{sheet}} = (12 \pm 1) \times 10^{-31}$ m^3/V^2 at the phonon resonance. Therefore, the $\chi^{(3)}$ value in graphene is 1 order of magnitude larger than in h-BN. This has important consequences for heterostructures made with graphene and h-BN, where the nonlinear optical behavior can be dominated by the graphene response.

To explore this result, we have built a graphene/h-BN heterostructure by transferring a monolayer graphene sample on top of fewlayer h-BN, following ref 43. In Figure 3, the CARS spectrum for a graphene/h-BN heterostructure is shown. The antiresonance line shape can be seen at the graphene phonon energy, while the resonant line shape at the h-BN phonon energy is not clearly resolved, despite the fact that the linear Raman spectrum (bottom plot) shows both phonon
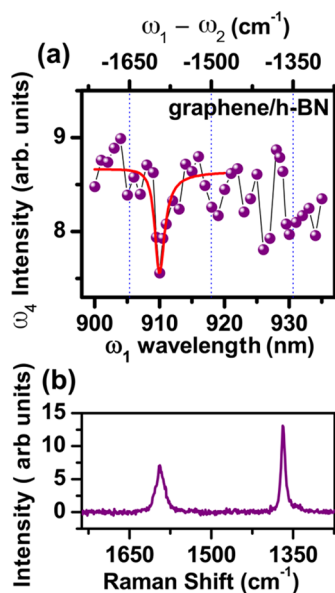
Figure 3. (a) CARS spectrum of a heterostructure formed by graphene on top of a fewlayer h-BN deposited on Si/SiO$_2$. The solid red lines are the fitted data using eq 1. (b) Raman spectrum of the same sample.

modes. Actually, the h-BN Raman peak (1366 cm^{-1}) is more intense than the graphene peak (1590 cm^{-1}); in contrast, the CARS signal is dominated by the graphene response due to its larger $\chi^{(3)}$ value. Finally, by using eq 1 to fit the experimental CARS spectrum near the graphene phonon energy, we have found $q = 0.1$, which is very similar to the case of graphene on top of quartz substrate. For this fitting we have used that final CARS intensity is the sum between the CARS intensity of graphene and h-BN; this is true if the band structures of both materials are not perturbed due to stacking. Since graphene on top of boron nitride in know to be a very clean sample, with low electron doping and high mobility,[3] this result implies that the antiresonance effect is robust in clean graphene samples and low doping levels compared to the results in quartz where the doping level is usually higher.[3]

In conclusion, we have measured the third-order optical nonlinear property of graphene, h-BN, and their heterostructure by coherent anti-Stokes Raman spectroscopy. The CARS intensity as a function of energy was modeled by a Fano line shape, which is shown to have good agreement with our experimental data. The observed anomalous antiresonance behavior for graphene and resonance behavior for h-BN was explained in terms of strong contribution arising form the available continuum of electronic states in graphene. This third-order behavior of graphene dominates the optical response of the heterostructure. We believe that our results provides new information for further development of theoretical works intended to describe the third-order nonlinear optical effects in these two-dimensional materials.

■ ASSOCIATED CONTENT

ⓢ Supporting Information

The Supporting Information is available free of charge on the ACS Publications website at DOI: 10.1021/acs.nanolett.7b00329.

Calculation procedure to extract the $\chi^{(3)}_{\text{sheet}}$ values for graphene and h-BN (PDF)

■ AUTHOR INFORMATION

Corresponding Author
*E-mail: lmalard@fisica.ufmg.br.

ORCID ⓘ
Thiago G. Mendes-de-Sa: 0000-0002-5027-462X
Leandro M. Malard: 0000-0003-4207-9653

Notes
The authors declare no competing financial interest.

■ REFERENCES

(1) Novoselov, K. S. Nobel Lecture: Graphene: Materials in the Flatland. *Rev. Mod. Phys.* **2011**, *83*, 837−849.

(2) Bonaccorso, F.; Sun, Z.; Hasan, T.; Ferrari, A. C. Graphene photonics and optoelectronics. *Nat. Photonics* **2010**, *4*, 611−622.

(3) Geim, A. K.; Grigorieva, I. V. Van der Waals heterostructures. *Nature* **2013**, *499*, 419−425.

(4) Xia, F.; Wang, H.; Xiao, D.; Dubey, M.; Ramasubramaniam, A. Two-dimensional material nanophotonics. *Nat. Photonics* **2014**, *8*, 899−907.

(5) Franken, P. A.; Hill, A. E.; Peters, C. W.; Weinreich, G. Generation of Optical Harmonics. *Phys. Rev. Lett.* **1961**, *7*, 118−119.

(6) Shen, Y. R. *The Principles of Nonlinear Optics*; Wiley Interscience: New York, 2003.

(7) Boyd, R. *Nonlinear optics*; Academic Press: London, 2008.

(8) Hendry, E.; Hale, P. J.; Moger, J.; Savchenko, A. K.; Mikhailov, S. A. Coherent Nonlinear Optical Response of Graphene. *Phys. Rev. Lett.* **2010**, *105*, 097401.

(9) Harutyunyan, H.; Beams, R.; Novotny, L. Controllable optical negative refraction and phase conjugation in graphite thin films. *Nat. Phys.* **2013**, *9*, 423−425.

(10) Hong, S.-Y.; Dadap, J. I.; Petrone, N.; Yeh, P.-C.; Hone, J.; Osgood, R. M. Optical Third-Harmonic Generation in Graphene. *Phys. Rev. X* **2013**, *3*, 021014.

(11) Li, Y.; Rao, Y.; Mak, K. F.; You, Y.; Wang, S.; Dean, C. R.; Heinz, T. F. Probing Symmetry Properties of Few-Layer MoS$_2$ and h-BN by Optical Second-Harmonic Generation. *Nano Lett.* **2013**, *13*, 3329−3333. PMID: 23718906.

(12) Kumar, N.; Najmaei, S.; Cui, Q.; Ceballos, F.; Ajayan, P. M.; Lou, J.; Zhao, H. Second harmonic microscopy of monolayer MoS$_2$. *Phys. Rev. B: Condens. Matter Mater. Phys.* **2013**, *87*, 161403.

(13) Malard, L. M.; Alencar, T. V.; Barboza, A. P. M.; Mak, K. F.; de Paula, A. M. Observation of intense second harmonic generation from MoS$_2$ atomic crystals. *Phys. Rev. B: Condens. Matter Mater. Phys.* **2013**, *87*, 201401.

(14) Ribeiro-Soares, J.; Janisch, C.; Liu, Z.; Elías, A. L.; Dresselhaus, M. S.; Terrones, M.; Cançado, L. G.; Jorio, A. Second Harmonic Generation in WSe$_2$. *2D Mater.* **2015**, *2*, 045015.

(15) Ciesielski, R.; Comin, A.; Handloser, M.; Donkers, K.; Piredda, G.; Lombardo, A.; Ferrari, A. C.; Hartschuh, A. Graphene Near-Degenerate Four-Wave Mixing for Phase Characterization of Broadband Pulses in Ultrafast Microscopy. *Nano Lett.* **2015**, *15*, 4968−4972. PMID: 26121487.

(16) Constant, T. J.; Hornett, S. M.; Chang, D. E.; Hendry, E. All-optical generation of surface plasmons in graphene. *Nat. Phys.* **2015**, *12*, 124−127.

(17) Woodward, R. I.; Murray, R. T.; Phelan, C. F.; de Oliveira, R. E. P.; Runcorn, T. H.; Kelleher, E. J. R.; Li, S.; de Oliveira, E. C.; Fechine, G. J. M.; Eda, G.; et al. Characterization of the second- and third-order nonlinear optical susceptibilities of monolayer MoS$_2$ using multiphoton microscopy. *2D Mater.* **2017**, *4*, 011006.

(18) Merano, M. Nonlinear optical response of a two-dimensional atomic crystal. *Opt. Lett.* **2016**, *41*, 187−190.

(19) Pope, I.; Payne, L.; Zoriniants, G.; Thomas, E.; Williams, O.; Watson, P.; Langbein, W.; Borri, P. Coherent anti-Stokes Raman scattering microscopy of single nanodiamonds. *Nat. Nanotechnol.* **2014**, *9*, 940−946.

(20) Opilik, L.; Schmid, T.; Zenobi, R. Modern Raman Imaging: Vibrational Spectroscopy on the Micrometer and Nanometer Scales. *Annu. Rev. Anal. Chem.* **2013**, *6*, 379−398.

(21) Huang, L.; Cheng, J.-X. Nonlinear Optical Microscopy of Single Nanostructures. *Annu. Rev. Mater. Res.* **2013**, *43*, 213−236.

(22) Kim, H.; Sheps, T.; Collins, P. G.; Potma, E. O. Nonlinear Optical Imaging of Individual Carbon Nanotubes with Four-Wave-Mixing Microscopy. *Nano Lett.* **2009**, *9*, 2991−2995.

(23) Mikhailov, S. Theory of the nonlinear optical frequency mixing effect in graphene. *Phys. E* **2012**, *44*, 924−927. The proceedings of the European Materials Research Symposium on Science and Technology of Nanotubes, Nanowires and Graphene.

(24) Cheng, J. L.; Vermeulen, N.; Sipe, J. E. Third-order nonlinearity of graphene: Effects of phenomenological relaxation and finite temperature. *Phys. Rev. B: Condens. Matter Mater. Phys.* **2015**, *91*, 235320.

(25) Rostami, H.; Polini, M. Theory of third-harmonic generation in graphene: A diagrammatic approach. *Phys. Rev. B: Condens. Matter Mater. Phys.* **2016**, *93*, 161411.

(26) Mikhailov, S. A. Quantum theory of the third-order nonlinear electrodynamic effects of graphene. *Phys. Rev. B: Condens. Matter Mater. Phys.* **2016**, *93*, 085403.

(27) Savostianova, N. A.; Mikhailov, S. A. Third harmonic generation from graphene lying on different substrates: optical-phonon resonances and interference effects. *Opt. Express* **2017**, *25*, 3268−3285.

(28) Malard, L.; Pimenta, M.; Dresselhaus, G.; Dresselhaus, M. Raman spectroscopy in graphene. *Phys. Rep.* **2009**, *473*, 51−87.

(29) Gorbachev, R. V.; Riaz, I.; Nair, R. R.; Jalil, R.; Britnell, L.; Belle, B. D.; Hill, E. W.; Novoselov, K. S.; Watanabe, K.; Taniguchi, T.; et al. Hunting for Monolayer Boron Nitride: Optical and Raman Signatures. *Small* **2011**, *7*, 465−468.

(30) Min, W.; Freudiger, C. W.; Lu, S.; Xie, X. S. Coherent Nonlinear Optical Imaging: Beyond Fluorescence Microscopy. *Annu. Rev. Phys. Chem.* **2011**, *62*, 507−530.

(31) Palomba, S.; Novotny, L. Nonlinear Excitation of Surface Plasmon Polaritons by Four-Wave Mixing. *Phys. Rev. Lett.* **2008**, *101*, 056802.

(32) Volkmer, A.; Cheng, J.-X.; Sunney Xie, X. Vibrational Imaging with High Sensitivity via Epidetected Coherent Anti-Stokes Raman Scattering Microscopy. *Phys. Rev. Lett.* **2001**, *87*, 023901.

(33) Cheng, J.-X.; Volkmer, A.; Xie, X. S. Theoretical and experimental characterization of coherent anti-Stokes Raman scattering microscopy. *J. Opt. Soc. Am. B* **2002**, *19*, 1363−1375.

(34) Liu, L.; Feng, Y. P.; Shen, Z. X. Structural and electronic properties of h -BN. *Phys. Rev. B: Condens. Matter Mater. Phys.* **2003**, *68*, 104102.

(35) Nestor, J.; Spiro, T. G.; Klauminzer, G. Spiro Coherent Anti-Stokes Raman Scattering (CARS) Spectra, with Resonance Enhancement, of Cytochrome c and Vitamin B_{12} in Dilute Aqueous Solution. *Proc. Natl. Acad. Sci. U. S. A.* **1976**, *73*, 3329−3332.

(36) Lotem, H.; Lynch, R. T.; Bloembergen, N. Interference between Raman resonances in four-wave difference mixing. *Phys. Rev. A: At., Mol., Opt. Phys.* **1976**, *14*, 1748−1755.

(37) Druet, S. A. J.; Attal, B.; Gustafson, T. K.; Taran, J. P. Electronic resonance enhancement of coherent anti-Stokes Raman scattering. *Phys. Rev. A: At., Mol., Opt. Phys.* **1978**, *18*, 1529−1557.

(38) Levenson, M. D.; Kano, S. S., Eds. *Introduction to Nonlinear Laser Spectroscopy (Revised ed.)*, revised ed.; Academic Press, 1988; p ii.

(39) Meier, T.; Schulze, A.; Thomas, P.; Vaupel, H.; Maschke, K. Signatures of Fano resonances in four-wave-mixing experiments. *Phys. Rev. B: Condens. Matter Mater. Phys.* **1995**, *51*, 13977−13986.

(40) Finkelstein-Shapiro, D.; Poulsen, F.; Pullerits, T. o.; Hansen, T. Coherent two-dimensional spectroscopy of a Fano model. *Phys. Rev. B: Condens. Matter Mater. Phys.* **2016**, *94*, 205137.

(41) Fano, U. Effects of Configuration Interaction on Intensities and Phase Shifts. *Phys. Rev.* **1961**, *124*, 1866−1878.

(42) Cheng, J. L.; Vermeulen, N.; Sipe, J. E. Third order optical nonlinearity of graphene. *New J. Phys.* **2014**, *16*, 053014.

(43) Cadore, A. R.; Mania, E.; Watanabe, K.; Taniguchi, T.; Lacerda, R. G.; Campos, L. C. Thermally activated hysteresis in high quality graphene/h-BN devices. *Appl. Phys. Lett.* **2016**, *108*, 233101.10.1063/1.4953162